32ND INTERNATIONAL COSMIC RAY CONFERENCE, BEIJING 2011

The average spatial density gradient of galactic cosmic rays and its temporal variation observed with the Global Muon Detector Network (GMDN)

M. KOZAI[1], K. MUNAKATA[1], C. KATO[1], S. YASUE[1], T. KUWABARA[2], J. W. BIEBER[2], P. EVENSON[2], M. ROCKENBACH[3], A. DAL LAGO[4], N. J. SCHUCH[5], M. TOKUMARU[6], M. L. DULDIG[7], J. E. HUMBLE[7], I. SABBAH[8], H. K. AL JASSAR[9], M. M. SHARMA[9], AND J. KOTA[10]

[1]*Physics Department, Shinshu University, Matsumoto, Nagano 390-8621, Japan.*
[2]*Bartol Research Institute and Department of Physics and Astronomy, University of Delaware, Newark, DE 19716, USA.*
[3]*Universidade do Vale do Paraíba(UNIVAP), 12244-000, São José dos Campos, SP, Brazil.*
[4]*National Institute for Space Research (INPE), 12227-010 São José dos Campos, SP, Brazil.*
[5]*Southern Regional Space Research Center (CRS/INPE), P.O. Box 5021, 97110-970, Santa Maria, RS, Brazil.*
[6]*Solar Terrestrial Environment Laboratory, Nagoya University, Nagoya, Aichi 464-8601, Japan.*
[7]*School of Mathematics and Physics, University of Tasmania, Hobart, Tasmania 7001, Australia.*
[8]*Department of Natural Sciences, College of Health Sciences, Public Authority of Applied Education and Training, Kuwait.*
[9]*Physics Department, Kuwait University, Kuwait 13060.*
[10]*Lunar and Planetary Laboratory, University of Arizona, Tucson, AZ 85721, USA.*
kmuna00@shinshu-u.ac.jp

Abstract: We deduce the spatial gradient of galactic cosmic rays in three dimensions from the fist order anisotropy observed with the Global Muon Detector Network. The anisotropy vector is first corrected for the solar wind convection and the Compton-Getting effect arising from the solar wind and the Earth's orbital motion around the Sun. We then convert the component anisotropy perpendicular to the interplanetary magnetic field to the spatial density gradient by assuming that the perpendicular anisotropy is mainly due to the diamagnetic streaming. In this paper, we analyze the solar cycle variation of the gradient observed with the GMDN during ten years between 2001 and 2010 and show that the derived density gradient is clearly decreasing with increasing solar activity toward the solar activity minimum in 2008-2009. We also find a clear seasonal variation in each of the radial and longitudinal component of the gradient vector in a close correlation with the heliographic latitude of the Earth. The amplitude of this seasonal variation also decreases with the increasing solar activity. We discuss the origin of this seasonal variation in terms of the global distribution of cosmic-ray density in the heliosphere.

Keywords: Diurnal anisotropy, Solar cycle variation of the cosmic-ray density gradient, Heliospheric modulation of galactic cosmic rays.

1 Introduction

The Galactic Cosmic Ray (GCR) intensity measured at the Earth changes with various time scales. The best-known 11-year variation in an anti-correlation with the 11-year solar activity cycle, which is typically observed in the neutron monitor counting rate, represents the variation of the GCR density (or omnidirectional intensity) at the Earth's orbit responding to the variation of the modulation parameters which governs the GCR transport into the heliosphere. The solar cycle variation of the modulation parameters also changes the spatial distribution of the GCR density in the vicinity of the Earth. The spatial distribution of the GCR density can be inferred from measuring the anisotropic streaming of GCRs at the Earth, as the diffusion streaming of GCRs reflects the local spatial gradient of the GCR density. This is an important objective of the Global Muon Detector Network (GMDN).

Data acquisition by the network began in December 1992, as two-hemisphere observations using a pair of muon detectors at Nagoya (Japan) and Hobart (Australia). Another small detector at Sao Martinho in Brazil was added to the network in March 2001 to fill a gap in directional coverage of the network over the Atlantic and Europe. The current GMDN was then completed in March 2006 by installing a new detector in Kuwait. The temporal variations of the density gradient in association with the Forbush decreases and corotating interaction regions have been analyzed using the observations with the GMDN [1, 2, 3]. In this paper, we analyze the solar cycle variation of the gradient ob-

served with the GMDN during ten years between 2001 and 2010.

2 Data analysis and results

We analyze the pressure corrected hourly count rate $I_{i,j}(t)$ of muons in the j-th directional channel of the i-th detector in the GMDN at the universal time t and derive three components ($\xi_x^{GEO}(t)$, $\xi_y^{GEO}(t)$, $\xi_z^{GEO}(t)$) of the first order anisotropy in the geographic (GEO) coordinate system by best-fitting the following model function to $I_{i,j}(t)$.

$$\begin{aligned} I_{i,j}^{fit}(t) = & \\ I_{i,j}^0(t) &+ \xi_x^{GEO}(t)(c_{1i,j}^1 \cos\omega t_i - s_{1i,j}^1 \sin\omega t_i) \\ &+ \xi_y^{GEO}(t)(s_{1i,j}^1 \cos\omega t_i + c_{1i,j}^1 \sin\omega t_i) \\ &+ \xi_z^{GEO}(t) c_{1i,j}^0 \end{aligned} \quad (1)$$

where $I_{i,j}^0(t)$ is a parameter representing the contributions from the omni-directional intensity and the atmospheric temperature effect, t_i is the local time at the i-th detector, $c_{1i,j}^1$, $s_{1i,j}^1$ and $c_{1i,j}^0$ are the coupling coefficients calculated by assuming the rigidity independent anisotropy with the response function of atmospheric muons to the primary cosmic rays ([4]) and $\omega = \pi/12$. In deriving the anisotropy vector $\boldsymbol{\xi}^{GEO}$, we also apply an analysis method which we developed to remove the atmospheric temperature effect from the derived anisotropy (see [1]). The correction for the temperature effect is of particular importance in analyzing the long-term temporal variation of $\boldsymbol{\xi}^{GEO}$.
The derived anisotropy is transformed to the heliocentric polar coordinate (HPC) system (r, θ, ϕ) and corrected for the solar wind convection anisotropy and the Compton-Getting anisotropy arising from the Earth's 30 km/s orbital motion around the Sun. For this correction, we use the solar wind velocity in the *ACE*-Level2 data and the Omni-data [5, 6]. We also use the *ACE* Interplanetary Magnetic Field (IMF) and solar wind data lagged by one hour, as a rough correction for the solar wind transit time between *ACE* and the Earth. We then divide the obtained diffusive anisotropy into components parallel and perpendicular to the IMF, as

$$\boldsymbol{\xi}(t) = \boldsymbol{\xi}_{\parallel}(t) + \boldsymbol{\xi}_{\perp}(t) \quad (2)$$

Figure 1 shows the magnitude of $\boldsymbol{\xi}_{\parallel}(t)$ averaged in each Carrington Rotation during ten years between 2001 and 2010. In spite of large fluctuations from one rotation to another, the thick black curve representing the central moving average over 14 rotations shows a clear long-term variation in which the magnitude of $\boldsymbol{\xi}_{\parallel}(t)$ decreases from the maximum in 2003 toward the minimum in 2009. This is an indication of the decrease of the GCR density gradient and/or parallel mean-free-path of the pitch-angle scattering of GCRs by the IMF fluctuation, as $\boldsymbol{\xi}_{\parallel}(t)$ is given by the product of these quantities.
Figure 2 shows the radial (r), longitudinal (ϕ) and latitudinal ($\pi/2 - \theta$) components of $\boldsymbol{\xi}_{\perp}(t)$ in the heliocentric polar coordinate system, each averaged over the *toward* (T)

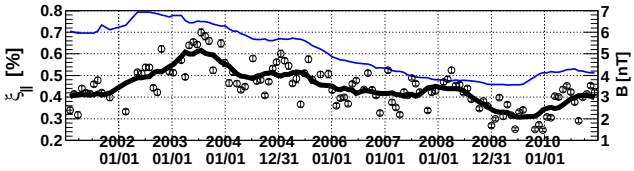

Figure 1: Observed diffusive anisotropy component parallel to the IMF. Each open circle displays the magnitude of $\boldsymbol{\xi}_{\parallel}(t)$ averaged over the Carrington Rotation. Errors are deduced from the dispersion of hourly values in each rotation. A thick black curve shows the central moving average of open circles over 14 rotations, while the thin curve displays the moving average of the IMF magnitude as an indicator of the solar activity.

and *away* (A) IMF sectors in every rotation. We define the IMF sector polarity based on the hourly mean IMF components in the heliocentric polar coordinate system, which are transformed from the GSE coordinate system used in *ACE*-Level2 and/or Omni-data. The sector polarity of the IMF vector ($\boldsymbol{B}$) is designated *toward* (T) if $B_{long} > B_r$ and *away* (A) if $B_r > B_{long}$. By assuming that $\boldsymbol{\xi}_{\perp}(t)$ in Figure 2 is predominantly due to the diamagnetic streaming (or the drift streaming) expressed by a vector product between the IMF vector and the density gradient vector, we can derive $\boldsymbol{G}_{\perp}(t)$ the fractional density gradient perpendicular to the IMF, as

$$\boldsymbol{G}_{\perp}(t) = \boldsymbol{b}(t) \times \boldsymbol{\xi}_{\perp}(t)/R_L(t) \quad (3)$$

where $\boldsymbol{b}(t)$ is the unit vector pointing in the IMF direction and $R_L(t)$ is the Larmor radius of protons with the effective energy which we set at 60 GeV, a representative median energy of GCRs observed with the GMDN. Figure 3 shows three components of $\boldsymbol{G}_{\perp}(t)$ in the same manner as Figure 2.
The negative (positive) $G_{\perp lat}(t)$ in T (A) sector in Figure 3 indicates the local maximum of the GCR density on the Heliospheric Current Sheet (HCS). This is qualitatively in accord with the drift model prediction for the density distribution during the "negative" polarity period of the solar polar magnetic field (also referred as the $A < 0$ epoch). In Figure 3, it is also clear that $G_{\perp lat}(t)$ decreases significantly from 2003 to 2008-2009 according to the solar activity decrease. A similar trend is also visible in $G_{\perp r}(t)$ or $G_{\perp long}(t)$, but is less evident partly due to the relatively smaller magnitude of these components. The long-term trend is less evident in $\boldsymbol{\xi}_{\perp}(t)$ in Figure 2 where from we derived $\boldsymbol{G}_{\perp}(t)$ in equation 3. This is due to $R_L(t)$ which increases with decreasing IMF magnitude compensating the decrease in $|\boldsymbol{G}_{\perp}(t)|$.

3 Discussion

One of the most notable features in Figure 3 is probably the significant seasonal variations seen in the radial and lon-

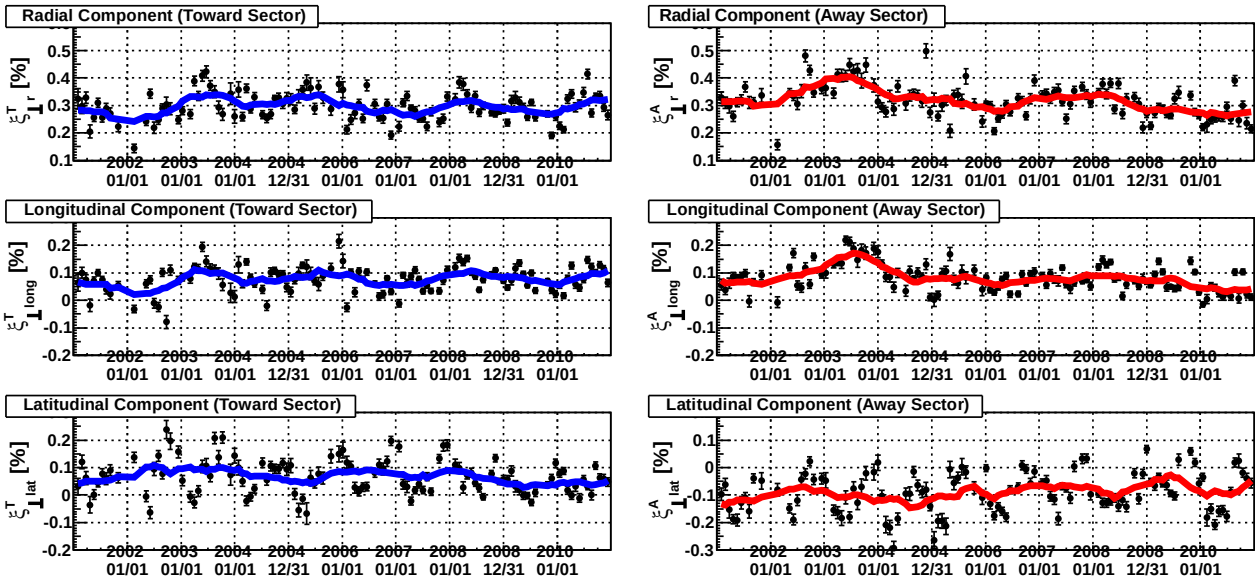

Figure 2: Observed diffusive anisotropy perpendicular to the IMF. Each solid circle in the left (right) panels shows the average component of $\boldsymbol{\xi}_\perp$ in the HPC in the *toward* (*away*) IMF sector in every rotation. The thick black curve in each panel represents the central moving average of the solid circles over 14 rotations.

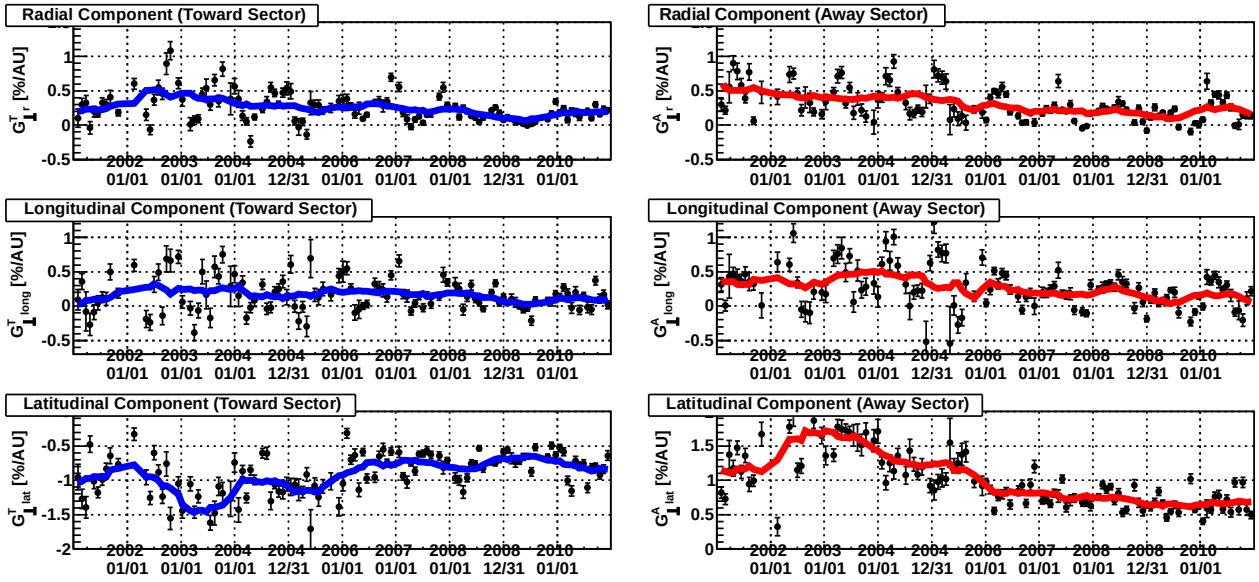

Figure 3: Derived density gradient perpendicular to the IMF. Solid circles in the left (right) panels display the rotation average of three components of $\boldsymbol{G}_\perp(t)$ in the T (A) IMF sector in every rotation. The thick curve in each panel represents the central moving average of the solid circles over 14 rotations.

gitudinal components ($G_{\perp r}(t)$ and $G_{\perp long}(t)$) of $\boldsymbol{G}_\perp(t)$ in Figure 3. As shown in Figure 4, the amplitude of this variation is as large as about 50 % of the yearly average of the gradient. The similar variation is also notable in the latitudinal component ($\xi_{\perp lat}(t)$) of $\boldsymbol{\xi}_\perp(t)$ in Figure 2 from which we derived $\boldsymbol{G}_\perp(t)$. To our knowledge, there is no other observation reporting such a significant seasonal variation of $\boldsymbol{G}_\perp(t)$ and the GMDN has discovered it for the first time. Although this is still preliminary, we confirm that the similar seasonal variation is also seen, with larger amplitude, in the gradient deduced from the observation by the Space Ship Earth (SSE) neutron monitor network, which monitors the intensity of GCRs with lower energy ($\sim$10 GeV) [7]. We now discuss this newly found seasonal variation of $\boldsymbol{G}_\perp(t)$.

It is clear in Figure 4 that the seasonal variations of $G_{\perp r}(t)$

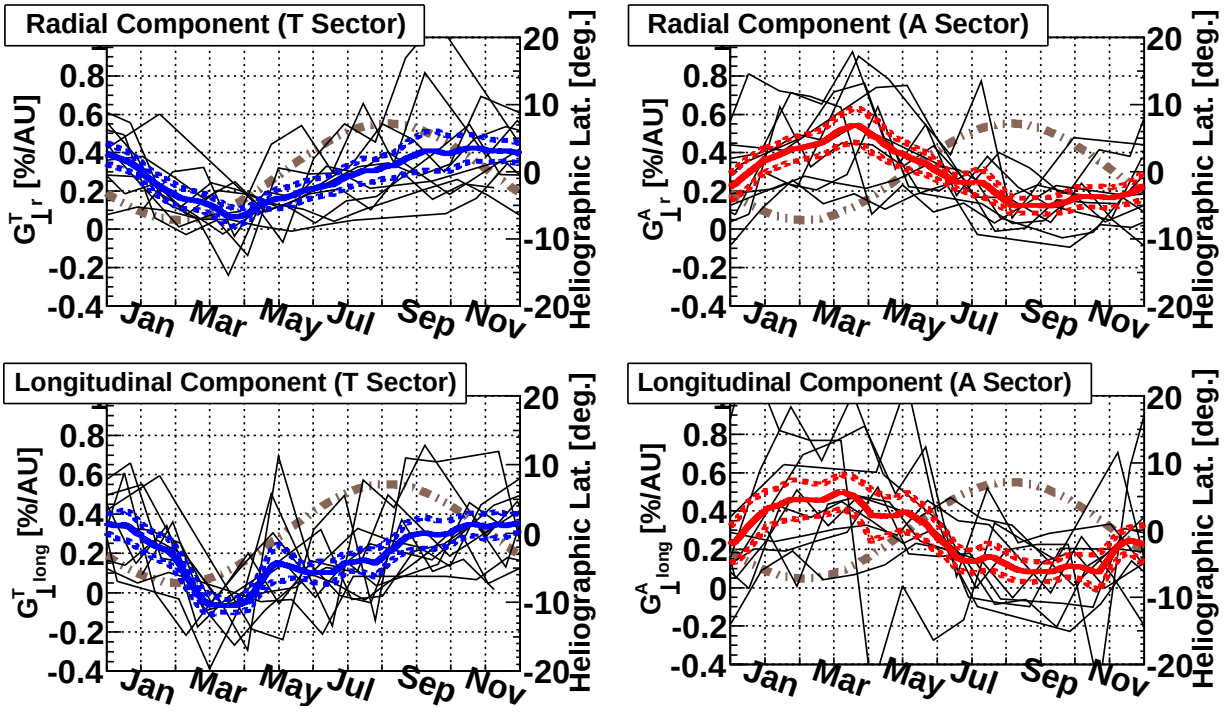

Figure 4: Average seasonal variations of $G_{\perp r}$ (top) and $G_{\perp long}$ (bottom). Thin black curves in each panel show the $G_{\perp r}$ ($G_{\perp long}$) in ten years between 2001 and 2010, while a thick solid curve displays the average of ten years. A pair of thick dotted curves in each panel indicates the error-range of the average deduced from the dispersion of thin curves. The left and right panels display the gradients in the T and A IMF sectors, respectively. The heliographic latitude of the Earth on the right vertical axis is also displayed by a thick chain-dotted curve in each panel.

and $G_{\perp long}(t)$ are in phase, while the variations in T and A sectors are out of phase to each other. Also seen in this figure is a close correlation between the gradient and the heliographic latitude of the Earth displayed by the thick chain-dotted curve in each panel. This correlation possibly suggests the seasonal variation arising from the latitude dependence of the GCR distribution which is organized along the wavy neutral sheet as the drift model predicts. According to our preliminary analyses based on the numerical simulation of GCR transport in a three-dimensional model heliosphere, it is possible to reproduce at least qualitatively the seasonal variation in Figure 4, if we assume the diffusion coefficients dependent on the heliographic latitude and decreasing near the equator. Deriving quantitative conclusions, however, requires closer comparison between the data and calculations which is now ongoing. We will also promote comparative analyses of the data from the GMDN and SSE to examine the energy dependence of the spatial distribution of GCR density in three dimensions.

4 Acknowledgments

This work is supported in part by NASA grant NNX 08AQ01G, in part by Grants-in-Aid for Scientific Research from the Ministry of Education, Culture, Sports, Science and Technology in Japan, and by the joint research programs of the Solar-Terrestrial Environment Laboratory, Nagoya University. The observations with the Kuwait Muon Telescope are supported by the Kuwait University grant SP03/03. We thank N. F. Ness for providing ACE magnetic field data via the ACE Science Center.

References

[1] Okazaki, Y. et al., Astrophys. J., 2008, **681**, 693-707
[2] Kuwabara, T. et al., Geophys. Res. Lett., 2004, **31**, L19803-1-L19803-5
[3] Kuwabara, T. et al., J. Geophys. Res., 2009, **114**, A05109-1-A05109-10
[4] Murakami, K., et al., IL Nuovo Cimento, 1979, **2C**, 635-651
[5] *ACE*-Level2 data are available at http://www.srl.caltech.edu/ACE/ASC/level2/index.html
[6] Omni-data are available at ftp://nssdcftp.gsfc.nasa.gov/spacecraft_sdata/omni/
[7] Bieber, J. W. et al., Astrophys. J., 2004, **601**, 103-106